THE JOURNAL OF PHYSICAL CHEMISTRY C
A JOURNAL OF THE AMERICAN CHEMICAL SOCIETY

pubs.acs.org/JPCC

Article

Re-Examining Open-Circuit Voltage in Dilute-Donor Organic Photovoltaics

Boya Zhang, Lakshmi N. S. Murthy, Aditya Mishra, Melanie H. Bowler, Chin-Lung Chung, Jia Du, Mihaela C. Stefan, Ken-Tsung Wong, Jason D. Slinker, and Julia W. P. Hsu*

Cite This: https://doi.org/10.1021/acs.jpcc.2c01814

Read Online

ACCESS | Metrics & More | Article Recommendations | Supporting Information

ABSTRACT: Dilute-donor (DD) organic photovoltaic (OPV) devices comprise a low concentration of donor molecules in an acceptor matrix. The open-circuit voltage (V_{oc}) of these devices is commonly higher than their bulk heterojunction (BHJ) counterparts and has been attributed to Schottky barrier heights between the anode and the acceptor matrix or reduced bimolecular recombination due to smaller donor/acceptor interfacial areas. Here, we examine the V_{oc} of a variety of small-molecule and polymer donors, all at 5 wt %, in both fullerene and non-fullerene acceptors by performing photovoltaic (PV) and electroluminescence (EL) measurements on the same devices. We find a substantial V_{oc} variation for different donors in the same acceptor matrix, indicating that DD V_{oc} cannot be adequately explained by the Schottky barrier or interfacial area. V_{oc} values of fullerene DD devices vary linearly with the band gap value as determined from the intercept of PV external quantum efficiency and EL spectra. In contrast, the non-fullerene acceptor (NFA) DD devices show V_{oc} variation with donors despite having the same band gap. These results show that V_{oc} of DD OPVs is predominantly determined by non-radiative voltage loss, similar to BHJ OPVs. NFA-based DD devices show promises for low voltage loss and high charge generation.

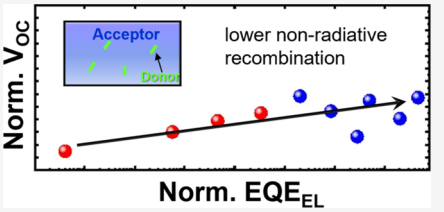

1. INTRODUCTION

Dilute donor (DD) organic photovoltaics (OPVs), which employ active layers consisting of a low concentration of donor molecules—typically < 10 wt %—in an acceptor matrix, show intriguing behaviors.[1−3,6] Notably, their short-circuit current density (J_{sc}) and open-circuit voltage (V_{oc}) can be as high as or higher than that of their bulk heterojunction (BHJ) counterparts.[1,2,4,5] Early reports found that V_{oc} in DD OPVs with fullerene acceptors can approach 1.0 V and be independent of the donor concentration.[1,2,6−8] While DD OPVs might not compete with the state-of-the-art BHJ OPVs based on non-fullerene acceptors (NFAs) in terms of power conversion efficiency (PCE), they provide a good platform to study fundamental device physics such as morphology effects on photocurrent generation and charge transport.[9−12] Furthermore, there have been only two publications on NFA DD devices;[13,14] hence, the difference between fullerene and NFA DD devices has not been studied.

This work focuses on understanding the factors that determine V_{oc} in DD OPVs. Previous explanations for the high V_{oc} in fullerene DD OPVs broadly fall into two categories: (1) V_{oc} corresponding to the Schottky contact barrier height between the anode and lowest unoccupied molecular orbital (LUMO) energy level of the acceptor[1,2,4,15] or (2) lower bimolecular recombination due to reduced donor−acceptor interfacial areas.[6] However, these studies related to the mechanism of Schottky barrier height relied solely on current density−voltage (J−V) measurements without an in-depth examination of the different loss mechanisms. While Vandewal et al.[6] was the first to examine V_{oc} and recombination loss, the paper focused on donor concentration dependence for a given donor and did not explain the V_{oc} difference for the two donors they studied. Recently, Benduhn et al.[7] have performed a comprehensive study of voltage losses in vacuum-deposited C_{60} systems; however, there has not been as much work on solution deposited DD systems, especially on systems employing NFAs. In this paper, we study DD systems with 5 wt % of various small-molecule (SM) and polymer donors embedded in both fullerene ([6,6]-phenyl-C71-butyric acid methyl ester ($PC_{71}BM$)) and non-fullerene (2,2′-((2Z,2′Z)-((12,13-bis(2-ethylhexyl)-3,9-diundecyl-12,13-dihydro-[1,2,5]-thiadiazolo[3,4-*e*]thieno[2″,3″:4′,5′]thieno[2′,3′:4,5]pyrrolo-[3,2-g]thieno[2′,3′:4,5]thieno[3,2-b]indole-2,10-diyl)bis-(methanylylidene))bis(5,6-difluoro-3-oxo-2,3-dihydro-1*H*-indene-2,1-diylidene))dimalononitrile (Y6)) acceptors. By performing electroluminescence (EL) and photovoltaic external quantum efficiency (EQE_{PV}) on the same device as recently done for BHJ systems,[7,16−18] voltage loss (ΔV) in these DD OPVs is examined. The broad range of solution-processable donor and acceptor materials investigated in this

Received: March 15, 2022
Revised: May 10, 2022

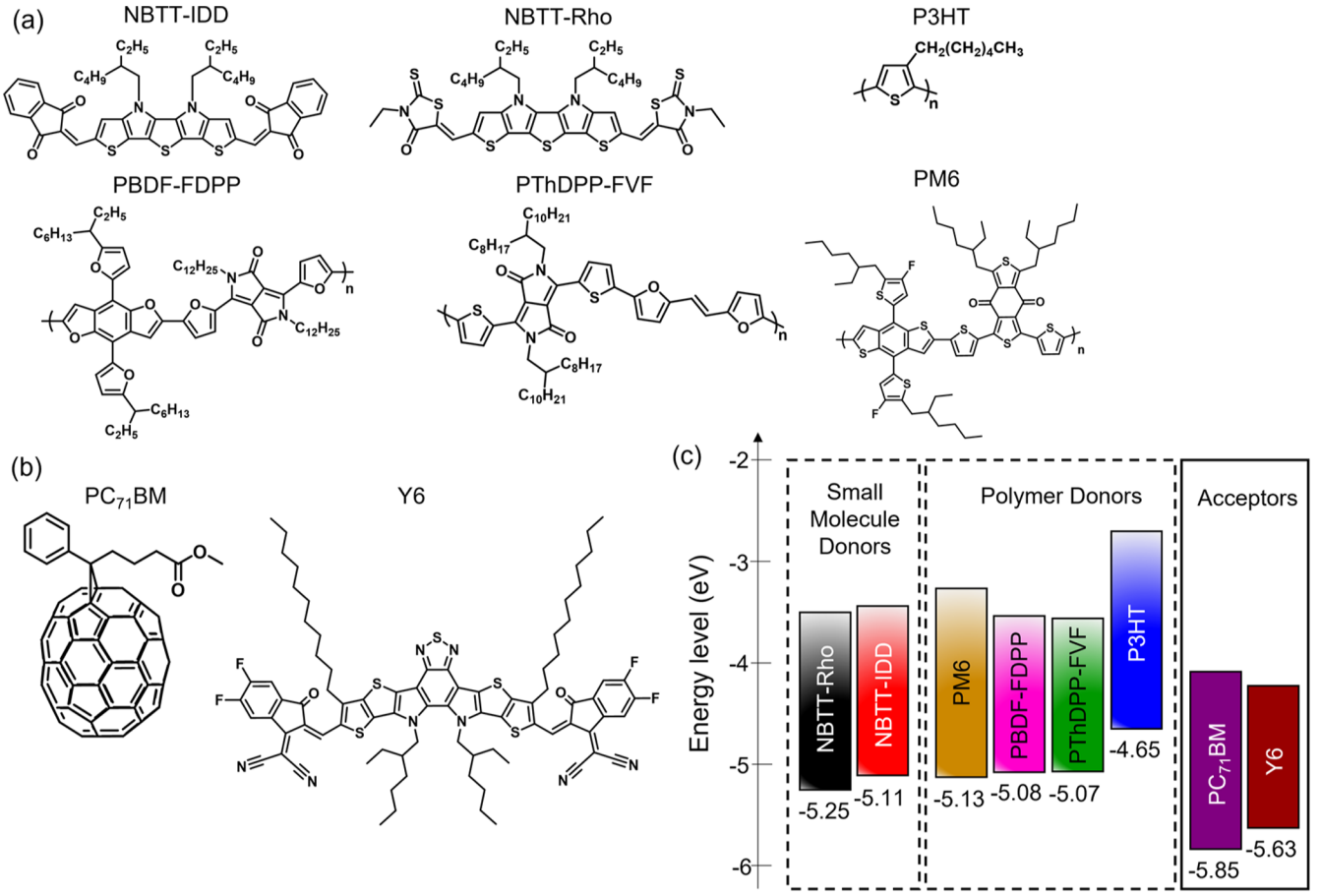

Figure 1. Chemical structures of (a) small-molecule (NBTT-IDD and NBTT-Rho) and polymer (PBDF-FDPP, PThDPP-FVF, PM6, and P3HT) donors and (b) acceptors ($PC_{71}BM$ and Y6). (c) Energy levels of donors and acceptors based on ionization energy (IE) determined from photoelectron spectroscopy in air (PESA) and E_g from Ultraviolet−Visible measurements (Table S1).

work will complement published vacuum-deposited fullerene work.

Because the voltage loss ΔV—the difference between the device V_{oc} and the band gap (E_g) or the charge-transfer (CT) state energy (E_{CT}) of the blend if $E_{CT} < E_g$—is substantially larger in OPVs compared to inorganic photovoltaics,[19] recently there have been active research focusing on understanding the limit of V_{oc} in OPVs.[16,18,20] The first possible voltage loss arises from the energy offset between donor and acceptor, resulting in E_{CT} smaller than E_g of the neat absorber, be it donor or acceptor. For OPVs based on fullerene acceptors, it was documented that the higher the E_{CT}, the higher the V_{oc}.[7,21,22] A large energy offset facilitates exciton dissociation, that is, higher J_{sc}, but with lower V_{oc}, hence the well-known V_{oc}−J_{sc} trade-off in fullerene BHJ OPVs.[23] Recently, highly efficient OPVs with little or no energy offsets have been reported in NFA systems,[24−27] resulting in E_{CT} similar to E_g. Nonetheless, other voltage losses remain.

Additional voltage losses can be separated into two parts: radiative (ΔV_R) and non-radiative (ΔV_{NR}) contributions (eq 1)[28,29]

$$\Delta V = \frac{E_g}{q} - V_{oc} = \left(\frac{E_g}{q} - V_{oc}^{rad}\right) + (V_{oc}^{rad} - V_{oc}) = \Delta V_R + \Delta V_{NR} \quad (1)$$

where q is the elementary charge. The radiative voltage loss is the difference between E_g/q and V_{oc}^{rad}, the V_{oc} when only radiative recombination occurs.[7] Here, we use E_g to represent the smaller E_{CT} or pure material's band gap. V_{oc}^{rad} is calculated from the device EQE_{PV} spectrum according to eq 2[30]

$$V_{oc}^{rad} = \frac{kT}{q} \ln\left(\frac{q\int_0^{+\infty} EQE_{PV}(E)\cdot\phi_{AM1.5G}(E)\cdot dE}{q\int_0^{+\infty} EQE_{PV}(E)\cdot\phi_{BB}(E)\cdot dE}\right) \quad (2)$$

where k is the Boltzmann constant, T is the temperature, $\emptyset_{AM1.5G}(E)$ is the one-sun spectrum at AM1.5G, and $\emptyset_{BB}(E)$ is the black-body spectrum at room temperature.

The rest of the voltage loss comes from non-radiative contribution, which is often the most dominant factor but is still not well understood, especially for NFA systems.[16,18,31] In eq 1, ΔV_{NR} is the difference between V_{oc}^{rad} and device V_{oc}. Because non-radiative recombination reduces EL efficiency, the reciprocity relationship allows us to directly obtain the non-radiative voltage loss by measuring EL external quantum efficiency (EQE_{EL}) using eq 3[19,28,32]

$$\Delta V_{NR} = \frac{kT}{q} \ln\left(\frac{1}{EQE_{EL}}\right) \quad (3)$$

Benduhn et al. showed that ΔV_{NR} decreases with increase in E_{CT} in fullerene-based OPVs, which is generally referred to as the "energy gap law" (EGL).[7] They attributed it to decrease in

https://doi.org/10.1021/acs.jpcc.2c01814
J. Phys. Chem. C XXXX, XXX, XXX−XXX

wave function overlap between the lowest CT state and vibrationally excited ground state, hence reducing non-radiative electron transfer rates. Interestingly, Saito et al. found that NFA BHJ OPVs with different ΔV_{NR} showed similar non-radiative recombination rates and proposed that the increase in the radiative rate could lead to higher EL efficiency and lower ΔV_{NR}.[16] Thus, the non-radiative recombination rate appears inadequate to explain ΔV_{NR} completely. Recently, it has been reported that ΔV_{NR} of NFA BHJ OPVs does not follow EGL; rather, it depends on the energy difference between CT and local exciton (LE) states, $\Delta E_{LE\text{-}CT}$. Hybridization occurs when the two energies are similar, resulting in higher CT state oscillator strength.[33] $\Delta E_{LE\text{-}CT}$ can be estimated from the smaller of the highest occupied molecular orbital (HOMO) or LUMO offset (ΔHOMO or ΔLUMO). A steep drop in ΔV_{NR} occurs as $\Delta E_{LE\text{-}CT}$ reaches zero and CT and LE states approach equilibrium.[17,18]

Here, we examine the V_{oc} of both SM and polymer donors at 5 wt % in $PC_{71}BM$ and Y6 acceptors and find a significant V_{oc} variation for different donors in the same acceptor matrix. It is surprising that such a low concentration of donors can affect photovoltage so significantly. These results reveal the inadequacy of our current understanding of the origin of DD OPV V_{oc}.

2. EXPERIMENTAL SECTION

2.1. Materials. Nitrogen-bridged terthiophene small molecules (NBTT-IDD and NBTT-Rho),[34,35] poly(4,8-bis(5-(2-ethylhexyl)furan-2-yl)benzo[1,2-*b*:4,5-*b*0]difuran-alt-2,5-didodecyl-3,6-di(furan-2-yl)pyrrolo[3,4-*c*]pyrrole-1,4(2*H*,5*H*)-dione) (PBDF-FDPP),[36] and poly(2,5-bis(2-decyltetradecyl)-3,6-di(thiophen-2-yl)pyrrolo[3,4-*c*]pyrrole-1,4(2*H*,5*H*)-dione-*b*-(*E*)-1,2-di(furan-2-yl)ethene) (PThDPP-FVF)[37] polymers were synthesized according to published literatures. Poly(3-hexylthiophene) (P3HT) was purchased from Rieke Metals, and poly[(2,6-(4,8-bis(5-(2-ethylhexyl-3-fluoro)thiophen-2-yl)-benzo[1,2-*b*:4,5-*b*′]dithiophene))-*alt*-(5,5-(1′,3′-di-2-thienyl-5′,7′-bis(2-ethylhexyl)benzo[1′,2′-*c*:4′,5′-*c*′]dithiophene-4,8-dione)] (PM6), Y6, and $PC_{71}BM$ were purchased from Lumtec. Chemical structures of all donors and acceptors investigated in this study are shown in Figure 1a,b.

2.2. Ultraviolet−Visible Absorption Spectroscopy. The absorbance spectra of thin films are measured using an Ocean Optics 4000 spectrometer with a DT-mini-2-GS light source. E_g values of neat donor and acceptor films are determined from Tauc plots of $(\alpha E)^2$ versus E for direct band gap materials (Figure S1), where α is the absorbance of thin films and E is the energy. E_g is estimated from the intersection point of the linear fits of the baseline and of the region where $(\alpha E)^2$ increases with increase in energy. The E_g values of neat donor and acceptor films are listed in Table S1.

2.3. Photoelectron Spectroscopy in Air. IE was measured using PESA (RKI instruments, AC2 model) with a deuterium lamp power of 100 nW. The resolution of PESA measurements is approximately 0.05 eV. The IEs of neat donor and acceptor films are listed in Table S1.

2.4. OPV Fabrication. Conventional devices are fabricated with a structure of glass/ITO/hole transport layer (HTL)/active layer/Ca/Al. Patterned ITO-coated glass substrates (Kintec, 15 Ω/sq) were rinsed with water, isopropanol, and acetone and then treated with UV Ozone (Procleaner Plus, Bioforce Nanoscience) for 20 min. Poly(3,4-ethylenedioxythiophene):poly(styrenesulfonate) (PEDOT:PSS) (Heraeus Clevios P VP.AI 4083, batch: 9006378404) was spin-coated onto precleaned ITO substrates at 4000 rpm for 30 s, followed by 170 °C annealing in N_2 for 5 min to form a 30 nm HTL. For $PC_{71}BM$ DD devices, donors and $PC_{71}BM$ with a total concentration of 20 mg/mL were dissolved overnight at 70 °C in chlorobenzene (Sigma-Aldrich) with 5 wt % donor concentrations. The active layers were made by spin-coating the prepared solutions at 1000 rpm for 60 s followed by annealing at 70 °C in N_2 for 10 min. The thickness of the active layer is approximately 65 nm. For Y6 DD devices, 5 wt % of NBTT-Rho, PBDF-FDPP, and PThDPP-FVF in Y6 with a total concentration of 10 mg/mL were dissolved overnight at 50 °C in chloroform (CF) (Sigma-Aldrich). The active layers were made by spin-coating the prepared solutions at 1000 rpm for 60 s, resulting in an active layer thickness of approximately 70 nm. For neat Y6 and 5 wt % PM6:Y6, a total concentration of 15 mg/mL in CF was stirred overnight at 50 °C. The active layer was made by spin-coating the prepared solutions at 950 and 850 rpm for 60 s, respectively, followed by annealing at 80 °C in N_2 for 10 min. The thickness of neat Y6 and 5 wt % PM6:Y6 is approximately 100 nm. Finally, 7 nm Ca and 100 nm Al were thermally evaporated (Angstrom Engineering) to complete the devices.

2.5. Current Density−Voltage (*J*−*V*) Measurements. The *J*−*V* measurements were performed in an N_2-filled glovebox under AM1.5G 100 mW/cm^2 illumination from a Class AAA solar simulator (Abet Technologies) using a low-noise sourcemeter (2635A, Keithley). The solar simulator intensity was calibrated using an NIST-traceable Si photodiode (Abet RR_227KG5). A 2.5 mm diameter aperture was placed in front of each device to define an illuminated area of 0.049 cm^2.

2.6. Photovoltaic External Quantum Efficiency Spectroscopy (EQE_{PV}). EQE_{PV} measurements were taken at short circuit using a monochromatic light from a tungsten halogen lamp (HORIBA TRIAX-180, grating 600 groove/mm) from 350 to 1000 nm. A chopper (Tetrahertz, C-995) was used to modulate the monochromatic light at 199 Hz, and a lock-in amplifier (Standard Research System, SR830) was used to demodulate the signal. Cutoff filters at 710 and 850 nm were used to reduce the scattered light from the light source so that we could measure the weak sub-band gap EQE_{PV} signals. EQE_{PV} measurements were quantified using an NREL-calibrated Si photodiode.

2.7. EL Spectroscopy. Luminance−current−voltage measurements were obtained with a 760D electrochemical analyzer from CH Instruments (Austin, TX) and a calibrated Labsphere integrating sphere with a thermoelectric cooled Si detector. The EL spectra were measured by an Ocean Optics model 0 Jaz spectrometer. EQE_{EL} measurements at constant current were obtained with a custom multiplexer testing station. This instrument supplied a constant current and measured the voltage with custom circuitry and simultaneously captured radiant flux with a calibrated Hamamatsu photodiode (S2387-1010R).

3. RESULTS AND DISCUSSION

To extract the V_{oc} values from the $PC_{71}BM$ and Y6 DD devices with different SM and polymer donors, we measure the *J*−*V* curves of neat $PC_{71}BM$, $PC_{71}BM$ DD devices with 5 wt % of different donors, neat Y6, and Y6 DD devices with 5 wt % of different donors under AM1.5G one-sun illumination (Figure

https://doi.org/10.1021/acs.jpcc.2c01814
J. Phys. Chem. C XXXX, XXX, XXX−XXX

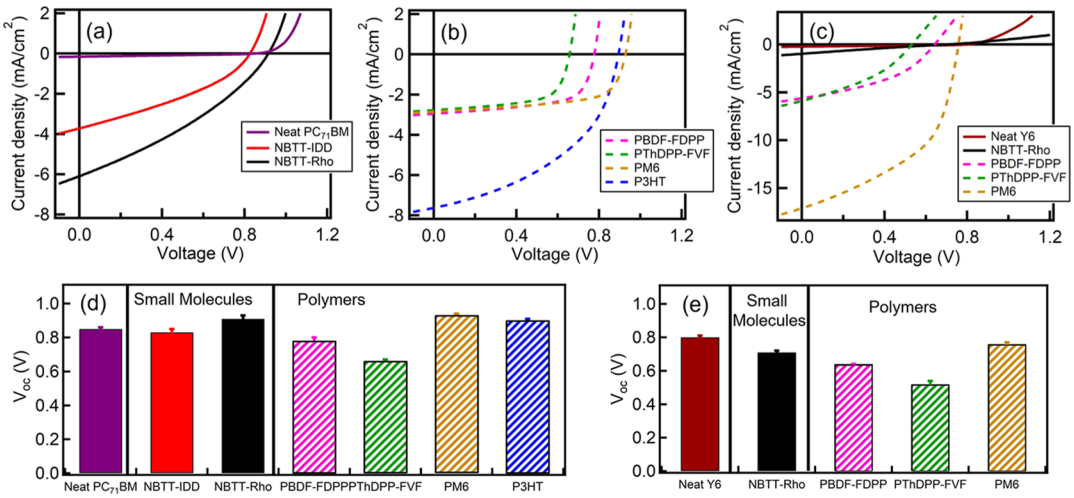

Figure 2. $J-V$ curves of (a) neat $PC_{71}BM$ (purple) and 5 wt % SM donor/$PC_{71}BM$ devices: NBTT-IDD (red) and NBTT-Rho (black), (b) 5 wt % polymer donor/$PC_{71}BM$ devices: PBDF-FDPP (pink), PThDPP-FVF (green), PM6 (gold), and P3HT (blue), and (c) neat Y6 (maroon solid line) and 5 wt % Y6 DD devices with SM donor NBTT-Rho (solid black line) and polymer donors (dashed lines): PBDF-FDPP (pink), PThDPP-FVF (green), and PM6 (gold). These $J-V$ curves are measured under one-sun AM1.5G 100 mW/cm^2 illumination and averaged over at least 5 diodes from different runs for each type. (d) V_{oc} values of neat $PC_{71}BM$ and 5 wt % (SM, polymer):$PC_{71}BM$ DD devices. (e) V_{oc} values of neat Y6 and 5 wt % (SM, polymer):Y6 DD devices. V_{oc} values are averaged over a minimum of 5 diodes from different runs, and the error bars represent standard deviations. Solid colors represent SM donors, and hatched patterns represent the polymer donors. The color schemes used in (d,e) are the same as in (a−c).

Table 1. Device Parameters of Neat Acceptors and 5 wt % of Different Donors in $PC_{71}BM$ (Top) or Y6 (Bottom) DD Devices[a]

sample		V_{oc} (V)	J_{sc} (mA/cm^2)	FF	PCE (%)
$PC_{71}BM$	neat acceptor	0.85 ± 0.01	0.16 ± 0.01	0.31 ± 0.01	0.04 ± 0.00
	NBTT-IDD	0.82 ± 0.02	3.70 ± 0.10	0.35 ± 0.01	1.08 ± 0.03
	NBTT-Rho	0.91 ± 0.01	6.07 ± 0.11	0.33 ± 0.00	1.86 ± 0.04
	PBDF-FDPP	0.77 ± 0.01	2.95 ± 0.11	0.63 ± 0.02	1.45 ± 0.08
	PThDPP-FVF	0.65 ± 0.01	2.77 ± 0.11	0.63 ± 0.03	1.16 ± 0.08
	PM6	0.92 ± 0.01	2.85 ± 0.15	0.63 ± 0.03	1.67 ± 0.13
	P3HT	0.89 ± 0.01	7.62 ± 0.12	0.45 ± 0.01	3.10 ± 0.08
Y6	neat acceptor	0.80 ± 0.01	0.24 ± 0.01	0.35 ± 0.01	0.07 ± 0.00
	NBTT-Rho	0.71 ± 0.01	0.97 ± 0.15	0.23 ± 0.01	0.16 ± 0.03
	PBDF-FDPP	0.64 ± 0.00	5.57 ± 0.55	0.41 ± 0.02	1.50 ± 0.22
	PThDPP-FVF	0.52 ± 0.02	5.75 ± 0.26	0.37 ± 0.01	1.12 ± 0.10
	PM6	0.76 ± 0.01	17.1 ± 0.5	0.49 ± 0.01	6.38 ± 0.33

[a]The standard deviations are calculated from at least 5 diodes from different runs.

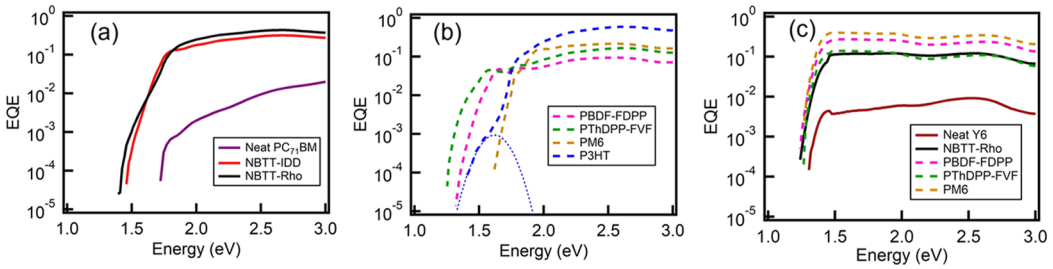

Figure 3. EQE_{PV} (in log scale) vs energy of (a) neat $PC_{71}BM$ and $PC_{71}BM$ DD devices with 5 wt % SM donors, (b) $PC_{71}BM$ DD devices with polymer donor, and (c) neat Y6 and Y6 DD devices. All color schemes used here are the same as in Figure 2. Solid lines represent neat acceptors and SM donors, and dashed lines represent polymer donors. The blue dotted curve in Figure 3b represents Gaussian fit to the true charge-transfer absorption in P3HT/$PC_{71}BM$ system with E_{CT} = 1.45 eV.

2a−c). The $J-V$ parameters are summarized in Table 1. The absorbance spectra show minimal differences between neat acceptor and DD films with 5 wt % of donor molecules (Figure S2), indicating that the photo-absorption is similar for all films and the exciton generation is predominantly in the acceptor matrix. However, Figure 2d,e shows that V_{oc} values for $PC_{71}BM$ and Y6 DD devices, respectively, with 5 wt % of different donors vary widely. While neat $PC_{71}BM$ device produces a V_{oc} of 0.85 V,[8,38] adding 5 wt % of NBTT-Rho and PM6 increases V_{oc} to above 0.9 V, while 5 wt % of PThDPP-

https://doi.org/10.1021/acs.jpcc.2c01814
J. Phys. Chem. C XXXX, XXX, XXX−XXX

Table 2. Energy and Voltage Values in Devices with Neat Acceptors and 5 wt % of Different Donors in $PC_{71}BM$ (Top) or Y6 (Bottom)[a]

sample		V_{oc} (V)	E_g^{int} (eV)	ΔV (V)[b]	V_{oc}^{rad} (V)[c]	ΔV_R (V)[d]	ΔV_{NR} (V)[e]
$PC_{71}BM$	neat acceptor	0.85 ± 0.01	1.83	0.98	1.42 ± 0.00	0.41	0.56 ± 0.00[e]
	NBTT-IDD	0.82 ± 0.02	1.62	0.80	1.35 ± 0.01	0.27	0.50 ± 0.01
	NBTT-Rho	0.91 ± 0.01	1.65	0.74	1.32 ± 0.01	0.33	0.40 ± 0.00
	PBDF-FDPP	0.77 ± 0.01	1.53	0.76	1.21 ± 0.00	0.32	0.42 ± 0.01
	PThDPP-FVF	0.65 ± 0.01	1.50	0.85	1.13 ± 0.00	0.37	0.47 ± 0.01
	PM6	0.92 ± 0.01	1.76	0.84	1.48 ± 0.00	0.28	0.54 ± 0.00
	P3HT	0.89 ± 0.01	1.77	0.88	1.32 ± 0.00	0.45	0.46 ± 0.01
Y6	neat acceptor	0.80 ± 0.01	1.39	0.59	1.09 ± 0.00	0.30	0.28 ± 0.00[f]
	NBTT-Rho	0.71 ± 0.01	1.41	0.70	1.09 ± 0.00	0.32	0.36 ± 0.00
	PBDF-FDPP	0.64 ± 0.00	1.42	0.78	1.08 ± 0.00	0.34	0.42 ± 0.01
	PThDPP-FVF	0.52 ± 0.02	1.41	0.89	1.09 ± 0.00	0.32	0.54 ± 0.01
	PM6	0.76 ± 0.01	1.40	0.64	1.08 ± 0.00	0.32	0.31 ± 0.00

[a] V_{oc} standard deviations are calculated from at least five diodes. The standard deviations of V_{oc}^{rad} and ΔV_{NR} are calculated from at least six diodes. [b] $E_g^{int}/q - V_{oc}$. [c] eq 2. [d] $E_g^{int}/q - V_{oc}^{rad}$. [e] Apply eq 3 using the EQE_{EL} value when injection current density equals J_{sc} unless otherwise noted. [f] For neat $PC_{71}BM$ and Y6 devices, the J_{sc} is too low to observe any EL signals, so ΔV_{NR} was calculated from the EQE_{EL} value measured at an injection current density of 18 and 46 mA/cm^2, respectively.

FVF in $PC_{71}BM$ lowers the V_{oc} to 0.65 V. Outside of this work, there was no published work on DD OPVs with solution-processable SM donors. V_{oc} values of various SM donors in C_{60} in vacuum-deposited DD devices are lower than those of neat C_{60} devices.[1,6,7] $PC_{71}BM$ DD devices with several polymer donors were previously reported to exhibit similar V_{oc}, leading to the proposal that V_{oc} of DD devices was determined by Schottky barrier height.[1,2,4,15] Our V_{oc} results shown in Figure 2d clearly indicate the incompleteness of previous studies. Figure 2e shows that similar to $PC_{71}BM$ DD devices, V_{oc} also varies substantially in Y6 DD devices, with PThDPP-FVF generating the lowest V_{oc} (0.52 V). Also notable is that both $PC_{71}BM$ and Y6 devices with 5 wt % PM6 can deliver the highest V_{oc} among all donors.

To study the voltage losses in these devices, EQE_{PV} spectra provide the necessary information for determining the maximum achievable V_{oc}, that is, V_{oc}^{rad}, according to eq 2. Figure 3 shows the EQE_{PV} spectra for devices made of neat acceptors as well as 5 wt % DDs. For $PC_{71}BM$ DD devices, adding donors produces EQE_{PV} signals below the E_g of $PC_{71}BM$ (~1.75 eV, Table S1) with the exception of PM6. However, only the P3HT DD device exhibits a clear CT state feature (blue curves in Figure 3b). In contrast, the PM6:$PC_{71}BM$ DD device and all Y6 DD devices display negligible absorption features below the acceptor band gap in the EQE_{PV} spectra.

Instead of fitting the EQE_{PV} spectra below the band gap with a Gaussian peak to determine E_{CT},[6,16] it was argued that a more accurate method to determine the E_{CT} value is from the intersection point of Gaussian fits to the normalized EQE_{PV} and EL spectra.[28,29] We apply this method to our $PC_{71}BM$ (Figure S3) and Y6 (Figure S4) DD devices and name the energy values at the intersection as E_g^{int} (Table 2).[22,38,39] For Y6 DD devices, because the drop-off of the EQE_{PV} signal is very steep (Figure 3c) with no discernible sub-band gap features, there are not as many decades in the EQE_{PV} data for accurate fitting. Therefore, we determine the characteristic energy values using three methods: the intersection method described above, the energy at half of EQE_{PV} maximum, and the energy at the maximum of the derivative of EQE_{PV}. Figure S4 shows that while there are systematic differences associated with the method used, the differences are small (≤ 0.04 eV). Most importantly, all donors produce similar characteristic energy values (difference ≤ 0.02 eV) when the data are analyzed using the same method. In Table 2, E_g^{int} values are determined using the intersection method for all devices.

However, the E_g^{int} values for these DD systems are not E_{CT}. The clearest evidence is seen in the 5 wt % P3HT:$PC_{71}BM$ device. Figure 3b shows a clear EQE_{PV} shoulder at 1.5 eV (blue curve). Fitting this region produces an E_{CT} value of 1.45 eV (blue dotted curve), which agrees with the published E_{CT} result for P3HT:$PC_{71}BM$ with different amounts of P3HT[8] and is different from the 1.77 eV E_g^{int} value obtained from the intersection method (Figure S3f). Thus, the EQE_{PV} signals below $PC_{71}BM$ E_g are not due to CT state absorption, but due to charge generation from excitons generated in the donor with a smaller band gap. For $PC_{71}BM$ systems, all donors except P3HT and PM6 have band gaps lower than or comparable to that of the acceptor. For Y6 DD devices, because Y6 is the smaller band gap (1.35 eV) component, we find the E_g^{int} value in these DD systems similar to the smaller E_g value of the neat donor or acceptor film (Table S1), that is, the energy difference between the ground state and the lowest singlet excited state. The circles in Figure 4 show a linear relationship between E_g^{int} and the smaller E_g value of the neat donor or acceptor (left y-axis). The solid black line in Figure 4

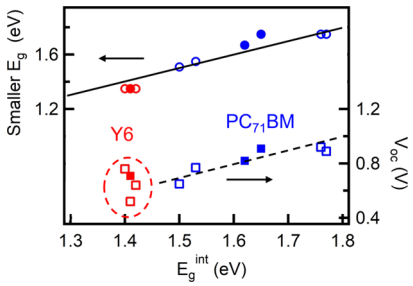

Figure 4. Smaller E_g of the neat donor or acceptor (circles, left y-axis) taken from Table S1 and V_{oc} (squares, right y-axis) as a function of E_g^{int} for $PC_{71}BM$ (blue) and Y6 (red) DD devices, determined from Figures S3 and S4, respectively. Solid (open) symbols represent SM (polymer) donors. The solid black line is E_g^{int} = smaller E_g and the dashed black line is $V_{oc} = E_g^{int}/q - 0.80$ V. The dashed red ellipse highlights the V_{oc} Y6 DD devices.

https://doi.org/10.1021/acs.jpcc.2c01814
J. Phys. Chem. C XXXX, XXX, XXX−XXX

represents E_g^{int} = smaller E_g and describes all $PC_{71}BM$ and Y6 DD devices well. This is because the lower band gap component dominates the EL emission. We do not see emissions from the CT state. It could be because the donor−acceptor interfacial area is so low that CT emission is too weak to be observed. However, we do observe emissions from the smaller-band gap donors in the $PC_{71}BM$ devices despite the concentration of donor materials being very low, suggesting that energy transfer from excitons created in $PC_{71}BM$ (larger band gap component) to the donor (smaller band gap component) is efficient in fullerene-based systems. Thus, the characteristic energy in these DD devices, as measured by the intersection of EQE_{PV} and EL spectra, is the energy gap of the neat component with the smaller band gap.

Blue squares in Figure 4 represent the V_{oc} of $PC_{71}BM$ DD devices (right y-axis), which show a linear dependence on E_g^{int} with a unity slope (black solid lines). In contrast, the V_{oc} values of Y6 DD devices (red squares inside dashed ellipse in Figure 4) vary with donors despite all having the same E_g^{int} values. The black dashed line in Figure 4 represents $V_{oc} = E_g^{int}/q - 0.8$ V. The offset between V_{oc} and E_g^{int} in our results is larger than that between V_{oc} and E_{CT} reported in Benduhn et al.,[7] most likely due to E_g^{int} values being larger than E_{CT} values. Figure S5 shows ΔV_{NR} versus E_g^{int} for all DD devices. $PC_{71}BM$ DD devices (blue symbols) exhibit a weak positive linear trend, while EGL would have predicted a negative linear correlation.[7,18,39] Y6 DD devices (red symbols) show a large ΔV_{NR} variation for the same E_g^{int}. Thus, we do not observe the EGL for either acceptor system. Again, this is most likely because E_g^{int} in our work is not E_{CT}.

Using EQE_{PV} spectra in Figure 3 and eq 2, V_{oc}^{rad} values are calculated for all DD OPVs (Table 2). ΔV_R values for most $PC_{71}BM$ DD devices are similar, ∼0.3 V; however, $PC_{71}BM$ DD devices with PThDPP-FVF and P3HT donors exhibit higher ΔV_R (0.37 and 0.45 V, respectively). In contrast, ΔV_R values are similar in neat Y6 and Y6 DD devices. There is no trend between ΔV_R and E_g^{int} (Figure S6). Thus, the V_{oc} variation for different donors in the same acceptor cannot be explained by ΔV_R.

Next, we examine non-radiative voltage losses. By performing EQE_{EL} measurements as a function of injection current density (Figure 5a,b), we obtain non-radiative voltage loss (ΔV_{NR}) according to eq 3. Very strikingly, a minute amount of donor (5 wt %) in the same acceptor matrix can alter the EL efficiency by almost 4 orders of magnitude. ΔV_{NR} values in Table 2 are determined for injected current density equal to J_{sc} under one-sun illumination.[40] For $PC_{71}BM$ DD devices, NBTT-Rho and PBDF-FDPP produce high EQE_{EL} and hence a small ΔV_{NR} of ∼0.4 V. $PC_{71}BM$ DD devices with P3HT and PThDPP-FVF polymer donors and NBTT-IDD SM donor exhibit lower EL, hence higher ΔV_{NR} of ∼0.5 V. PM6 is an outlier; while it has the largest ΔV_{NR} in $PC_{71}BM$ (0.54 V) because its E_g^{int} is large (1.76 eV) and ΔV_R is small (0.28 V), its V_{oc} is not significantly suppressed. For Y6 DD devices, the EL efficiency (Figure 5b) directly reflects the DD OPV V_{oc} with the highest PM6 and the lowest PThDPP-FVF.

To examine whether V_{oc} of DD devices is governed by non-radiative voltage loss for all DD systems, we normalize the V_{oc} (y-axis) and EQE_{EL} (x-axis) of the DD devices by those of the corresponding neat acceptor because the neat-acceptor devices have different V_{oc} and EQE_{EL}. Figure 5c shows that the two normalized quantities exhibit a linear correlation (dashed black line), signaling that V_{oc} is determined by ΔV_{NR}. Thus, similar

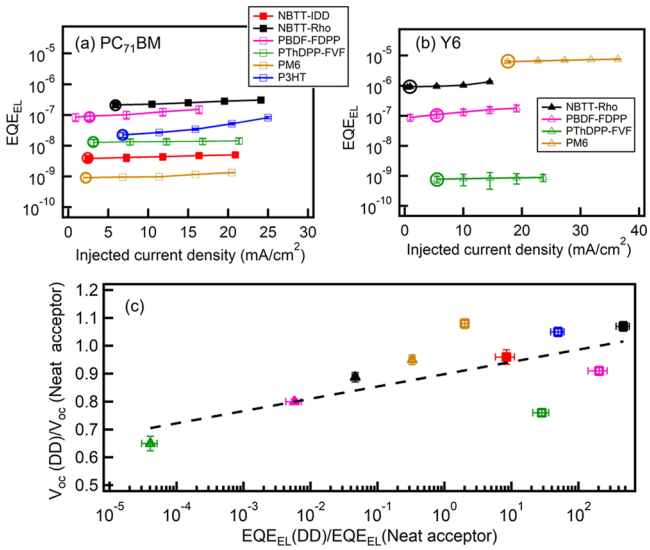

Figure 5. EQE_{EL} vs injected current density of (a) $PC_{71}BM$ and (b) Y6 DD devices with 5 wt % donors; SM donors are represented by filled symbols and polymer donors by open symbols. The color schemes used here are the same as in Figure 2. Circles in (a,b) indicate the EQE_{EL} values at which the injected current density is equal to the J_{sc} of the device under one-sun illumination. (c) $V_{oc}(DD)/V_{oc}$ (neat acceptor) as a function of the EQE_{EL} ratio between DD and the neat acceptor for all $PC_{71}BM$ and Y6 DD devices. Error bars represent standard deviations over at least six diodes.

to BHJ OPVs, non-radiative voltage loss is the determining factor for V_{oc} in DD OPVs.[7,41] This result is independent of the acceptor being fullerene or non-fullerene. Figure 5c indicates that the previous attribution of DD V_{oc} to Schottky junction barrier height is misguided. Some factors might have contributed to this flawed explanation. First, early works examined limited numbers of donors.[1,15] For example, if one only examined our results for SM donors in $PC_{71}BM$ (Figure 2d), they would think V_{oc} is independent of donors. For donor materials with similar structures or chemistry, they will interact similarly with the acceptor, leading to comparable charge recombination rates and non-radiative voltage loss; therefore, V_{oc} values would appear independent of donors. Furthermore, for many fullerene acceptor systems, for example, P3HT:$PC_{71}BM$, BHJ V_{oc} is much lower than that for DD OPVs for the same donor−acceptor pair.[2,8,42] Thus, compared to BHJ, the V_{oc} variation in DD OPVs seems to be negligible. By examining a wider variety of donors in fullerene and NFA acceptors, we show here that a low concentration of donors does affect V_{oc} quite significantly, largely determined by non-radiative loss.

$J-V$ results (Figure 2b and Table 1) show that P3HT generates the highest J_{sc} (7.62 mA/cm^2) among $PC_{71}BM$ DD devices, and PM6 generates the highest J_{sc} (17.1 mA/cm^2) among Y6 DD devices. Both systems exhibit high V_{oc} (0.89 V for P3HT in $PC_{71}BM$ and 0.76 V for PM6 in Y6). The J_{sc} variation cannot be explained by variation in the donor−acceptor interfacial area because the donor concentration is kept fixed at 5 wt % or photo-absorption because all donors in the same acceptor exhibit similar absorption spectra (Figure S2). While P3HT:PCBM has been extensively studied,[43−46] PM6:Y6 is new and intriguing. BHJ studies indicated that there is little or no energy offset between donors and Y6.[18,26,27] As

https://doi.org/10.1021/acs.jpcc.2c01814
J. Phys. Chem. C XXXX, XXX, XXX−XXX

shown above, E_g^{int} values are the same for all Y6 devices because their EQE_{PV} and EL spectra exhibit the same shape (Figures 3c and S4), which are determined by Y6 (the smaller band gap component) and are independent of the donor's chemical or electronic properties. Thus, V_{oc}^{rad} and the radiative loss for the different Y6 DD OPVs are all similar. However, they do exhibit different V_{oc} values and different ΔV_{NR} (Figures 2e and 5b and Table 2). For example, 5 wt % PThDPP-FVF in Y6 produces a V_{oc} 0.24 V lower than 5 wt % PM6 in Y6, 0.52 V versus 0.76 V, clearly deviating from the EGL (Figure 4). ΔV_{NR} for PThDPP-FVF:Y6 is 0.54 V, and for PM6:Y6 it is 0.31 V. These results indicate that the intramolecular morphology and interaction, which are not accounted for in the analysis so far, might play a critical role in determining both non-radiative voltage loss and charge generation. Karki et al. argued that the PM6:Y6 system has a well-defined interface and no contact between Y6's acceptor moieties and PM6's backbones, which could explain the reduced recombination rate.[26] Recently, it has been argued that the non-radiative voltage loss is related to the hybridization of CT and LE states in NFA systems.[33] Figure 6 displays ΔV_{NR} values for our Y6 DD devices versus $\Delta E_{LE\text{-}CT}$ along with those of the Y6 BHJ devices taken from this work and the literature.[18,26] We use the smaller ΔHOMO or ΔLUMO between the donor and Y6, with energy level values determined from cyclic voltammetry measurements of neat materials, to represent $\Delta E_{LE\text{-}CT}$, which is the practice in the literature.[17,18] The same general trends of ΔV_{NR} versus $\Delta E_{LE\text{-}CT}$ between BHJ and DD indicate that the hybridization between CT and LE states is responsible for V_{oc} OPVs based on Y6 NFA.

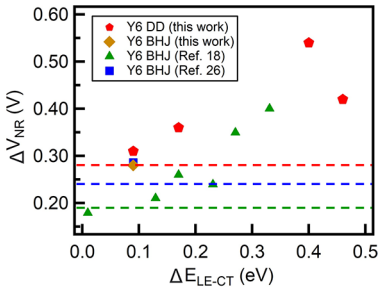

Figure 6. ΔV_{NR} vs $\Delta E_{LE\text{-}CT}$ (Table S2, smaller ΔHOMO or ΔLUMO between donor and Y6) for Y6 devices. The ΔV_{NR} values from this work are shown in red pentagons (DD) and brown diamonds (BHJ). The data with green triangles and blue squares are obtained from the literature.[18,26] Dashed red lines denote the ΔV_{NR} for neat Y6 obtained from this work (0.28 V). Dashed blue (0.24 V)[26] and green (0.19 V)[18] lines are from the literature.

4. CONCLUSIONS

By examining a wide variety of SM and polymer donors in both $PC_{71}BM$ and Y6 acceptors, we find that a low concentration (5 wt %) of donors can affect the V_{oc} greatly. Consequently, the previously proposed Schottky junction formation as the explanation for high V_{oc} observed in fullerene DD systems was flawed. Through combined photovoltaic and EL studies, our results unambiguously show that V_{oc} of DD OPVs is dictated by non-radiative voltage loss, similar to BHJ OPVs. While V_{oc} values of the $PC_{71}BM$-based DD systems follow the EGL, those of the Y6-based NFA DD systems do not. Hence, for $PC_{71}BM$-based DD OPVs, V_{oc} can be increased by using a larger band gap donor. Going beyond fullerene systems to NFA-based DD OPVs, the strategies to maximize DD V_{oc} are similar to those for BHJ OPVs: applying molecular design to optimize the pairing of donor and acceptor for low bimolecular recombination and matching CT and LE energy levels. The simultaneous high V_{oc} and J_{sc} observed for 5 wt % PM6:Y6 DD devices show great promises in exploring NFA DD systems.

■ ASSOCIATED CONTENT

Supporting Information

The Supporting Information is available free of charge at https://pubs.acs.org/doi/10.1021/acs.jpcc.2c01814.

Tauc plots of neat donor and acceptor films, absorption spectra, determination of E_g^{int} of $PC_{71}BM$ and Y6 DD devices, ΔV_{NR} versus E_g^{int}, and ΔV_R versus E_g^{int} plots for $PC_{71}BM$ and Y6 DD devices (PDF)

■ AUTHOR INFORMATION

Corresponding Author

Julia W. P. Hsu − *Department of Materials Science and Engineering, University of Texas at Dallas, Richardson, Texas 75080, United States;* orcid.org/0000-0002-7821-3001; Email: jwhsu@utdallas.edu

Authors

Boya Zhang − *Department of Materials Science and Engineering, University of Texas at Dallas, Richardson, Texas 75080, United States*

Lakshmi N. S. Murthy − *Department of Materials Science and Engineering, University of Texas at Dallas, Richardson, Texas 75080, United States*

Aditya Mishra − *Department of Materials Science and Engineering, University of Texas at Dallas, Richardson, Texas 75080, United States*

Melanie H. Bowler − *Department of Physics, University of Texas at Dallas, Richardson, Texas 75080, United States;* orcid.org/0000-0001-5058-2852

Chin-Lung Chung − *Department of Chemistry, National Taiwan University, Taipei 10617, Taiwan*

Jia Du − *Department of Chemistry, University of Texas at Dallas, Richardson, Texas 75080, United States*

Mihaela C. Stefan − *Department of Chemistry, University of Texas at Dallas, Richardson, Texas 75080, United States;* orcid.org/0000-0003-2475-4635

Ken-Tsung Wong − *Department of Chemistry, National Taiwan University, Taipei 10617, Taiwan; Institute of Atomic and Molecular Science, Academic Sinica, Taipei 10617, Taiwan;* orcid.org/0000-0002-1680-6186

Jason D. Slinker − *Department of Materials Science and Engineering, University of Texas at Dallas, Richardson, Texas 75080, United States; Department of Physics, University of Texas at Dallas, Richardson, Texas 75080, United States;* orcid.org/0000-0001-7338-586X

Complete contact information is available at: https://pubs.acs.org/10.1021/acs.jpcc.2c01814

Author Contributions

B.Z. and L.N.S.M. contributed equally. B.Z. and L.N.S.M.: conceptualization, methodology, data curation, formal analysis, investigation, manuscript-writing. A.M. and M.H.B.: EL measurements, data curation. C.-L.C. and J.D.: synthesis of donor materials. M.C.S., K.-T.W., and J.D.S.: funding

https://doi.org/10.1021/acs.jpcc.2c01814
J. Phys. Chem. C XXXX, XXX, XXX−XXX

acquisition, resources, and manuscript—review and editing. J.W.P.H.: conceptualization, supervision, methodology, funding acquisition, resources, manuscript—review and editing, and project management.

Notes

The authors declare no competing financial interest.

■ ACKNOWLEDGMENTS

We thank W. Xu for performing photoluminescence measurements on neat materials. This project was supported by the National Science Foundation (CBET-1916612, ECCS-1906505, CHE-1566059, and CHE-1609880), UT Dallas Spring 2020 Seed Program for Interdisciplinary Research (SPIRe) Grant, Welch Foundation (AT-1740), and Ministry of Science and Technology Taiwan (MOST 107-2113-M-002-019-MY3 and 110-2628-M-A49-001-MY3). M.C.S. thanks the generous endowed chair support from the Eugene McDermott Foundation. J.W.P.H. acknowledges the Texas Instruments Distinguished Chair in Nanoelectronics.

■ REFERENCES

(1) Zhang, M.; Wang, H.; Tian, H.; Geng, Y.; Tang, C. W. Bulk Heterojunction Photovoltaic Cells with Low Donor Concentration. *Adv. Mater.* **2011**, *23*, 4960−4964.

(2) Yang, B.; Xiao, Z.; Huang, J. Polymer Aggregation Correlated Transition from Schottky-Junction to Bulk Heterojunction Organic Solar Cells. *Appl. Phys. Lett.* **2014**, *104*, 143304.

(3) Ding, K.; Liu, X.; Forrest, S. R. Charge Transfer and Collection in Dilute Organic Donor-Acceptor Heterojunction Blends. *Nano Lett.* **2018**, *18*, 3180−3184.

(4) Yang, B.; Guo, F.; Yuan, Y.; Xiao, Z.; Lu, Y.; Dong, Q.; Huang, J. Solution-Processed Fullerene-Based Organic Schottky Junction Devices for Large-Open-Circuit-Voltage Organic Solar Cells. *Adv. Mater.* **2013**, *25*, 572−577.

(5) Zheng, Y.-q.; Potscavage, W. J.; Komino, T.; Hirade, M.; Adachi, J.; Adachi, C. Highly Efficient Bulk Heterojunction Photovoltaic Cells Based on C_{70} and Tetraphenyldibenzoperiflanthene. *Appl. Phys. Lett.* **2013**, *102*, 143304.

(6) Vandewal, K.; Widmer, J.; Heumueller, T.; Brabec, C. J.; McGehee, M. D.; Leo, K.; Riede, M.; Salleo, A. Increased Open-Circuit Voltage of Organic Solar Cells by Reduced Donor-Acceptor Interface Area. *Adv. Mater.* **2014**, *26*, 3839−3843.

(7) Benduhn, J.; Tvingstedt, K.; Piersimoni, F.; Ullbrich, S.; Fan, Y.; Tropiano, M.; McGarry, K. A.; Zeika, O.; Riede, M. K.; Douglas, C. J.; Barlow, S.; Marder, S. R.; Neher, D.; Spoltore, D.; Vandewal, K. Intrinsic Non-Radiative Voltage Losses in Fullerene-Based Organic Solar Cells. *Nat. Energy* **2017**, *2*, 17053.

(8) Xu, L.; Wang, J.; Villa, M. d. A.; Daunis, T. B.; Lee, Y.-J.; Malko, A. V.; Hsu, J. W. P. Quantitative Analyses of Competing Photocurrent Generation Mechanisms in Fullerene-Based Organic Photovoltaics. *J. Phys. Chem. C* **2016**, *120*, 16470−16477.

(9) Spoltore, D.; Hofacker, A.; Benduhn, J.; Ullbrich, S.; Nyman, M.; Zeika, O.; Schellhammer, S.; Fan, Y.; Ramirez, I.; Barlow, S.; Riede, M.; Marder, S. R.; Ortmann, F.; Vandewal, K. Hole Transport in Low-Donor-Content Organic Solar Cells. *J. Phys. Chem. Lett.* **2018**, *9*, 5496−5501.

(10) Song, Y.; Schubert, A.; Liu, X.; Bhandari, S.; Forrest, S. R.; Dunietz, B. D.; Geva, E.; Ogilvie, J. P. Efficient Charge Generation via Hole Transfer in Dilute Organic Donor-Fullerene Blends. *J. Phys. Chem. Lett.* **2020**, *11*, 2203−2210.

(11) Albes, T.; Xu, L.; Wang, J.; Hsu, J. W. P.; Gagliardi, A. Origin of Photocurrent in Fullerene-Based Solar Cells. *J. Phys. Chem. C* **2018**, *122*, 15140−15148.

(12) Jiang, W.; Jin, H.; Stolterfoht, M.; Shaw, P. E.; Nagiri, R. C. R.; Kopidakis, N.; Burn, P. L. Loss Mechanisms in Fullerene-Based Low-Donor Content Organic Solar Cells. *J. Phys. Chem. C* **2018**, *122*, 20611−20618.

(13) Liu, Y.; Zhang, J.; Zhou, G.; Liu, F.; Zhu, X.; Zhang, F. Electric Field Facilitating Hole Transfer in Non-Fullerene Organic Solar Cells with a Negative HOMO Offset. *J. Phys. Chem. C* **2020**, *124*, 15132−15139.

(14) Yao, N.; Wang, J.; Chen, Z.; Bian, Q.; Xia, Y.; Zhang, R.; Zhang, J.; Qin, L.; Zhu, H.; Zhang, Y.; Zhang, F. Efficient Charge Transport Enables High Efficiency in Dilute Donor Organic Solar Cells. *J. Phys. Chem. Lett.* **2021**, *12*, 5039−5044.

(15) Sutty, S.; Williams, G.; Aziz, H. Fullerene-Based Schottky-Junction Organic Solar Cells: A Brief Review. *J. Photon. Energy* **2014**, *4*, 040999.

(16) Saito, T.; Natsuda, S.-i.; Imakita, K.; Tamai, Y.; Ohkita, H. Role of Energy Offset in Nonradiative Voltage Loss in Organic Solar Cells. *Sol. RRL* **2020**, *4*, 2000255.

(17) Classen, A.; Chochos, C. L.; Lüer, L.; Gregoriou, V. G.; Wortmann, J.; Osvet, A.; Forberich, K.; McCulloch, I.; Heumüller, T.; Brabec, C. J. The Role of Exciton Lifetime for Charge Generation in Organic Solar Cells at Negligible Energy-Level Offsets. *Nat. Energy* **2020**, *5*, 711−719.

(18) Chen, X.-K.; Qian, D.; Wang, Y.; Kirchartz, T.; Tress, W.; Yao, H.; Yuan, J.; Hülsbeck, M.; Zhang, M.; Zou, Y.; Sun, Y.; Li, Y.; Hou, J.; Inganäs, O.; Coropceanu, V.; Bredas, J.-L.; Gao, F. A Unified Description of Non-Radiative Voltage Losses in Organic Solar Cells. *Nat. Energy* **2021**, *6*, 799−806.

(19) Rau, U.; Blank, B.; Müller, T. C. M.; Kirchartz, T. Efficiency Potential of Photovoltaic Materials and Devices Unveiled by Detailed-Balance Analysis. *Phys. Rev. Appl.* **2017**, *7*, 044016.

(20) Xie, Y.; Wu, H. Balancing Charge Generation and Voltage Loss toward Efficient Nonfullerene Organic Solar Cells. *Mater. Today Adv.* **2020**, *5*, 100048.

(21) Graham, K. R.; Erwin, P.; Nordlund, D.; Vandewal, K.; Li, R.; Ngongang Ndjawa, G. O.; Hoke, E. T.; Salleo, A.; Thompson, M. E.; McGehee, M. D.; Amassian, A. Re-Evaluating the Role of Sterics and Electronic Coupling in Determining the Open-Circuit Voltage of Organic Solar Cells. *Adv. Mater.* **2013**, *25*, 6076−6082.

(22) Ullbrich, S.; Benduhn, J.; Jia, X.; Nikolis, V. C.; Tvingstedt, K.; Piersimoni, F.; Roland, S.; Liu, Y.; Wu, J.; Fischer, A.; Neher, D.; Reineke, S.; Spoltore, D.; Vandewal, K. Emissive and Charge-Generating Donor−Acceptor Interfaces for Organic Optoelectronics with Low Voltage Losses. *Nat. Mater.* **2019**, *18*, 459−464.

(23) Scharber, M. C.; Mühlbacher, D.; Koppe, M.; Denk, P.; Waldauf, C.; Heeger, A. J.; Brabec, C. J. Design Rules for Donors in Bulk-Heterojunction Solar Cells—Towards 10 % Energy-Conversion Efficiency. *Adv. Mater.* **2006**, *18*, 789−794.

(24) Liu, J.; Chen, S.; Qian, D.; Gautam, B.; Yang, G.; Zhao, J.; Bergqvist, J.; Zhang, F.; Ma, W.; Ade, H.; Inganäs, O.; Gundogdu, K.; Gao, F.; Yan, H. Fast Charge Separation in a Non-Fullerene Organic Solar Cell with a Small Driving Force. *Nat. Energy* **2016**, *1*, 16089.

(25) Qian, D.; Zheng, Z.; Yao, H.; Tress, W.; Hopper, T. R.; Chen, S.; Li, S.; Liu, J.; Chen, S.; Zhang, J.; Liu, X.-K.; Gao, B.; Ouyang, L.; Jin, Y.; Pozina, G.; Buyanova, I. A.; Chen, W. M.; Inganäs, O.; Coropceanu, V.; Bredas, J.-L.; Yan, H.; Hou, J.; Zhang, F.; Bakulin, A. A.; Gao, F. Design Rules for Minimizing Voltage Losses in High-Efficiency Organic Solar Cells. *Nat. Mater.* **2018**, *17*, 703−709.

(26) Karki, A.; Vollbrecht, J.; Dixon, A. L.; Schopp, N.; Schrock, M.; Reddy, G. N. M.; Nguyen, T. Q. Understanding the High Performance of over 15% Efficiency in Single-Junction Bulk Heterojunction Organic Solar Cells. *Adv. Mater.* **2019**, *31*, No. e1903868.

(27) Yuan, J.; Zhang, Y.; Zhou, L.; Zhang, G.; Yip, H.-L.; Lau, T.-K.; Lu, X.; Zhu, C.; Peng, H.; Johnson, P. A.; Leclerc, M.; Cao, Y.; Ulanski, J.; Li, Y.; Zou, Y. Single-Junction Organic Solar Cell with over 15% Efficiency Using Fused-Ring Acceptor with Electron-Deficient Core. *Joule* **2019**, *3*, 1140−1151.

(28) Vandewal, K.; Tvingstedt, K.; Gadisa, A.; Inganäs, O.; Manca, J. V. Relating the Open-Circuit Voltage to Interface Molecular

https://doi.org/10.1021/acs.jpcc.2c01814
J. Phys. Chem. C XXXX, XXX, XXX−XXX

Properties of Donor:Acceptor Bulk Heterojunction Solar Cells. *Phys. Rev. B: Condens. Matter Mater. Phys.* **2010**, *81*, 125204.
(29) Vandewal, K.; Benduhn, J.; Nikolis, V. C. How to Determine Optical Gaps and Voltage Losses in Organic Photovoltaic Materials. *Sustainable Energy Fuels* **2018**, *2*, 538−544.
(30) Wang, Y.; Qian, D.; Cui, Y.; Zhang, H.; Hou, J.; Vandewal, K.; Kirchartz, T.; Gao, F. Optical Gaps of Organic Solar Cells as a Reference for Comparing Voltage Losses. *Adv. Energy Mater.* **2018**, *8*, 1801352.
(31) Liu, S.; Yuan, J.; Deng, W.; Luo, M.; Xie, Y.; Liang, Q.; Zou, Y.; He, Z.; Wu, H.; Cao, Y. High-Efficiency Organic Solar Cells with Low Non-Radiative Recombination Loss and Low Energetic Disorder. *Nat. Photonics* **2020**, *14*, 300−305.
(32) Kirchartz, T.; Rau, U. Detailed Balance and Reciprocity in Solar Cells. *Phys. Status Solidi A* **2008**, *205*, 2737−2751.
(33) Eisner, F. D.; Azzouzi, M.; Fei, Z.; Hou, X.; Anthopoulos, T. D.; Dennis, T. J. S.; Heeney, M.; Nelson, J. Hybridization of Local Exciton and Charge-Transfer States Reduces Nonradiative Voltage Losses in Organic Solar Cells. *J. Am. Chem. Soc.* **2019**, *141*, 6362−6374.
(34) Wang, Q. Solution-Processed Small-Molecule Organic Solar Cells. Ph.D. Dissertation; Eindhoven University of Technology, 2020.
(35) Kaiser, W.; Murthy, L. N. S.; Chung, C. L.; Wong, K. T.; Hsu, J. W. P.; Gagliardi, A. Origin of Hole Transport in Small Molecule Dilute Donor Solar Cells. *Adv. Energy Sustain. Res.* **2021**, *2*, 2000042.
(36) Du, J.; Fortney, A.; Washington, K. E.; Biewer, M. C.; Kowalewski, T.; Stefan, M. C. Benzo[1,2-b:4,5-b']difuran and Furan Substituted Diketopyrrolopyrrole Alternating Copolymer for Organic Photovoltaics with High Fill Factor. *J. Mater. Chem. A* **2017**, *5*, 15591−15600.
(37) Du, J.; Bulumulla, C.; Mejia, I.; McCandless, G. T.; Biewer, M. C.; Stefan, M. C. Evaluation of (E)-1,2-di(furan-2-yl)ethene as Building Unit in Diketopyrrolopyrrole Alternating Copolymers for Transistors. *Polym. Chem.* **2017**, *8*, 6181−6187.
(38) Murthy, L. N. S.; Kramer, A.; Zhang, B.; Su, J.-M.; Chen, Y.-S.; Wong, K.-T.; Vandenberghe, W. G.; Hsu, J. W. P. Energy Levels in Dilute-Donor Organic Solar Cell Photocurrent Generation: A Thienothiophene Donor Molecule Study. *Org. Electron.* **2021**, *92*, 106137.
(39) Vandewal, K.; Gadisa, A.; Oosterbaan, W. D.; Bertho, S.; Banishoeib, F.; Van Severen, I.; Lutsen, L.; Cleij, T. J.; Vanderzande, D.; Manca, J. V. The Relation between Open-Circuit Voltage and the Onset of Photocurrent Generation by Charge-Transfer Absorption in Polymer: Fullerene Bulk Heterojunction Solar Cells. *Adv. Funct. Mater.* **2008**, *18*, 2064−2070.
(40) Rau, U. Reciprocity Relation between Photovoltaic Quantum Efficiency and Electroluminescent Emission of Solar Cells. *Phys. Rev. B: Condens. Matter Mater. Phys.* **2007**, *76*, 085303.
(41) Azzouzi, M.; Kirchartz, T.; Nelson, J. Factors Controlling Open-Circuit Voltage Losses in Organic Solar Cells. *Trends Chem.* **2019**, *1*, 49−62.
(42) Xu, L.; Wang, J.; Hsu, J. W. P. Structural Order: The Dominant Factor for Nongeminate Recombination in Organic Photovoltaic Devices. *J. Phys. Chem. C* **2017**, *121*, 9242−9248.
(43) Nieuwendaal, R. C.; Ro, H. W.; Germack, D. S.; Kline, R. J.; Toney, M. F.; Chan, C. K.; Agrawal, A.; Gundlach, D.; VanderHart, D. L.; Delongchamp, D. M. Measuring Domain Sizes and Compositional Heterogeneities in P3HT-PCBM Bulk Heterojunction Thin Films with ^{1}H Spin Diffusion NMR Spectroscopy. *Adv. Funct. Mater.* **2012**, *22*, 1255−1266.
(44) Ko, S.; Hoke, E. T.; Pandey, L.; Hong, S.; Mondal, R.; Risko, C.; Yi, Y.; Noriega, R.; McGehee, M. D.; Brédas, J.-L.; Salleo, A.; Bao, Z. Controlled Conjugated Backbone Twisting for an Increased Open-Circuit Voltage While Having a High Short-Circuit Current in Poly(Hexylthiophene) Derivatives. *J. Am. Chem. Soc.* **2012**, *134*, 5222−5232.
(45) Van Bavel, S. S.; Bärenklau, M.; De With, G.; Hoppe, H.; Loos, J. P3HT/PCBM Bulk Heterojunction Solar Cells: Impact of Blend Composition and 3D Morphology on Device Performance. *Adv. Funct. Mater.* **2010**, *20*, 1458−1463.
(46) Balderrama, V. S.; Estrada, M.; Viterisi, A.; Formentin, P.; Pallarés, J.; Ferré-Borrull, J.; Palomares, E.; Marsal, L. F. Correlation between P3HT Inter-Chain Structure and Jsc of P3HT:PC[70]BM Blends for Solar Cells. *Microelectron. Reliab.* **2013**, *53*, 560−564.

https://doi.org/10.1021/acs.jpcc.2c01814
J. Phys. Chem. C XXXX, XXX, XXX−XXX